5-17-2014

Contrasting Environments Associated with Storm Prediction Center Tornado Outbreak Forecasts using Synoptic-Scale Composite Analysis

Alyssa Victoria Bates

Contrasting environments associated with Storm Prediction Center tornado outbreak forecasts using synoptic-scale composite analysis

By

Alyssa Victoria Bates

A Thesis
Submitted to the Faculty of
Mississippi State University
in Partial Fulfillment of the Requirements
for the Degree of Master of Science
in Geosciences (Professional Meteorology/Climatology)
in the Department of Geosciences

Mississippi State, Mississippi

May 2014

Contrasting environments associated with Storm Prediction Center tornado outbreak forecasts using synoptic-scale composite analysis

By

Alyssa Victoria Bates

Approved:

_____

Andrew E. Mercer
(Major Professor)

_____

P. Grady Dixon
(Committee Member)

_____

Michael E. Brown
(Committee Member/Graduate Coordinator)

_____

R. Gregory Dunaway
Professor and Dean
College of Arts & Sciences

Name: Alyssa Victoria Bates

Date of Degree: May 17, 2014

Institution: Mississippi State University

Major Field: Geosciences

Major Professor: Dr. Andrew E. Mercer

Title of Study: Contrasting environments associated with Storm Prediction Center tornado outbreak forecasts using synoptic-scale composite analysis

Pages in Study: 51

Candidate for Degree of Master of Science

Tornado outbreaks have significant human impact, so it is imperative forecasts of these phenomena are accurate. As a synoptic setup lays the foundation for a forecast, synoptic-scale aspects of Storm Prediction Center (SPC) outbreak forecasts of varying accuracy were assessed. The percentages of the number of tornado outbreaks within SPC 10% tornado probability polygons were calculated. False alarm events were separately considered. The outbreaks were separated into quartiles using a point-in-polygon algorithm. Statistical composite fields were created to represent the synoptic conditions of these groups and facilitate comparison. Overall, temperature advection had the greatest differences between the groups. Additionally, there were significant differences in the jet streak strengths and amounts of vertical wind shear. The events forecasted with low accuracy consisted of the weakest synoptic-scale

setups. These results suggest it is possible that events with weak synoptic setups should be regarded as areas of concern by tornado outbreak forecasters.

DEDICATION

I would like to dedicate this thesis to my mother, Vicki Bates, my brother Dylan, Nancy and Tony Peters, Sandee and Russell Dougherty, and Alicia Klees.

ACKNOWLEDGEMENTS

The author expresses her sincerest gratitude to the people without whom this thesis could not have been completed. First and foremost, I would like to profusely thank Dr. Andrew E. Mercer, my thesis advisor, for his unwavering guidance and advice. I would also like to thank Dr. P. Grady Dixon and Dr. Michael E. Brown for their guidance and helpful suggestions. And finally, I would like to thank Andy Dean from the Storm Prediction Center for supplying the tornado probability dataset.

TABLE OF CONTENTS

DEDICATION ii

ACKNOWLEDGEMENTS iii

LIST OF TABLES v

LIST OF FIGURES vi

CHAPTER

I. INTRODUCTION 1

Proposed Research Questions and Hypothesis 2
Previous Literature on Data 2
Previous Literature on Tornado Outbreaks 4
Definition and Classification 4
Case Studies 5
Forecasting 7
Compositing 8
Purpose of this Research 9

II. DATA AND METHODS 11

Data 11
Methods 12

III. RESULTS AND DISCUSSION 23

IV. SUMMARY AND CONCLUSIONS 39

BIBLIOGRAPHY 44

APPENDIX

A LIST OF EVENT DATES 50

LIST OF TABLES

1 Sea Level Pressure Correlation Matrix 31

2 Temperature Advection Correlation Matrix 31

3 Specific Humidity (kg kg^{-1}) for All Timesteps and QFs 31

4 Surface Temperature Correlation Matrix 32

5 Surface Specific Humidity Correlation Matrix 32

6 Event Dates Organized by QF 51

LIST OF FIGURES

1 Example Event with Moderate Risk and 10% Tornado Probability 18

2 Illustration of Buffer Methodology 18

3 Illustration of Buffered Polygon (orange) versus the Original (brown)..... 19

4 Percentage of Tornado Reports inside SPC 10% Tornado Probabliity Polygons with Quartiles Identified 19

5 Sample Events from Each QF 20

6 Example Dendrogram Used to Determine 4 Map Types for Q2..... 21

7 Sample Map Types from Q4 of 500 hPa Height (m) at 24 Hours before Outbreak Time 22

8 Examples of Trough Orientations from Q2..... 32

9 Example of Q4 500 mb Heights (m)..... 33

10 SLP (hPa) from Most Representative Map Type at Outbreak Time for Each QF..... 34

11 Temperature Advection (K s^{-1}) 6 Hours Prior to Outbreak at 850 hPa for Each QF..... 35

12 300 hPa Wind Speeds (m s^{-1}, solid lines) and Height (m, dashed lines) at Outbreak Time for Q4 Map Type 2..... 36

13 300 hPa Wind Speeds (m s^{-1}) at Outbreak Time for Q1 and Q3..... 36

14 Differential Vorticity Advection (s^{-2} Pa^{-1}, shaded) and Height (m, solid lines) at 500 hPa for Each QF..... 37

15 850-300 hPa Vertical Wind Shear (m s^{-1}) for Q1 and Q4..... 38

16 Number of Events per Season for Each QF..... 43

CHAPTER I

INTRODUCTION

Tornado outbreaks have been impacting the United States for centuries. However, they are becoming more problematic with recent economic inflation. In 1974, the “Super Outbreak” of April 3–4 included 48 killer tornadoes that took 335 lives (Corfidi et al. 2010). More recently, the “historic” April 27, 2011 outbreak resulted in 316 fatalities and over $4.2 billion in damages (Hayes 2011). With 199 tornadoes, it was the largest single-day outbreak on record (Blunden and Arndt 2012). It is imperative measures are taken to prevent disasters of this magnitude from causing such a tremendous negative impact. One such measure is to improve tornado outbreak forecasts. Recent research suggests the current methods of tornado outbreak forecasting could be improved (Hitchens and Brooks 2012). By improving these forecasts, people can be warned of inclement weather on the order of hours, rather than the minutes tornado warnings provide. As synoptic-scale processes give a broad picture of tornado outbreak favorability, this project seeks to aid in this effort by finding limitations in their forecasts by assessing the differences between the synoptic-scale setups of events with forecasts of varying accuracy.

Proposed Research Questions and Hypothesis

This study sought to determine whether or not there are significant synoptic-scale differences between SPC-forecasted outbreaks of varying accuracy. It is believed there will be such differences between these groups. The null hypothesis is the events' synoptic setups will not be significantly different.

Previous Literature on Data

Although the earliest tornado reports are found in Finley (1887), official tornado reporting did not begin until 1954 (Brooks et al. 2003, Kelly et al. 1978). As tornado intensity started being analyzed (Fujita 1981), Kelly et al. (1978) created a tornado climatology from 1950–1976 that included analyses of diurnal cycles and tornado intensity (Brooks et al. 2003). In 1987, the climatology was expanded to include reports from as early as 1916 (Fujita 1987, Brooks et al. 2003).

The reliability of the tornado report dataset has been questioned in several studies (Kelly et al. 1978, Doswell and Burgess 1988, Brooks et al. 2003, Verbout et al. 2006, Doswell 2007, others). This is partially because tornadoes used to be reported by "relatively untrained witnesses" (Doswell and Burgess 1988, Verbout et al. 2006). Doswell and Burgess (1988) also call the spatial and temporal accuracy of the reports into question due to reporting errors and variability in their collection for warning verification (Verbout et al. 2006). In addition, operational changes, such as changes in damage survey procedures, have been cited as some of the dataset's limitations (Verbout et al. 2006).

The most challenging limitation of the dataset is the increase in the number of tornado reports over time. In fact, the number of reported tornadoes has almost doubled since the 1950s (Brooks et al. 2003, Verbout et al. 2006, Shafer and Doswell 2009). This is due to many factors, most of which are non-meteorological (Brooks et al. 2003, Doswell et al. 2006—hereafter D06, Doswell 2007). These factors include various secular developments, such as population increases, increased public awareness, the implementation of National Weather Services offices and spotter networks, and the advancement of Doppler radar (Brooks et al. 2003, Verbout et al. 2006). However, these factors will not have a significant impact on this study, as it is focusing on groups of recent tornado outbreaks rather than individual historical events.

Several methods have been developed to attempt to circumvent this population bias. As stated in D06, a popular method is to detrend the reports using linear regression (Verbout et al. 2006). D06 argued the standard linear regression only accounts for the number of tornadoes; therefore, they performed a regression on only the top 30 tornado days per year. Then, they performed the same regression on the synoptic-scale variables associated with tornado development in order to incorporate more parameters than just the number of reports (D06). Shafer and Doswell (2010a) and Shafer and Doswell (2011) also employed this method in their studies that worked on ranking, classifying, and discriminating between tornado outbreaks.

Previous Literature on Tornado Outbreaks

Definition and Classification

No formal definition exists for a tornado outbreak. The most basic definition, from the American Meteorological Society *Glossary of Meteorology*, calls an outbreak "multiple tornado occurrences within a single synoptic-scale system" (Glickman 2000). Researchers expand upon this to create a definition to suit their purposes. Some (Pautz 1969, Galway 1977, Cook and Schaefer 2008) define them using only a number of tornadoes, while others (Hagemeyer 1997, Edwards et al. 2004, D06, Verbout et al. 2006) include other parameters with their definitions. Some go a step further and argue there should be no formal definition since the perception of an "outbreak" varies spatially and temporally (Edwards et al. 2004, D06, Verbout et al. 2006, Corfidi 2013). The present study will define an outbreak based on the criterion outlined in D06.

The work in D06 stems from Thompson and Vescio (1998)'s attempt to rank tornado outbreaks by incorporating tornado intensity, path width, and path length into one index, termed the Destruction Potential Index (DPI). Though no literature exists on its limitations and it is still being used (Cook and Schaefer 2008), Edwards et al. (2004) decided to improve upon the DPI. This study devised an index, termed the O index, to rank tornado outbreaks from 1970–2002. It consisted of a weighted linear combination of variables including: the number of tornadoes on that day, the number of violent (F4 and F5 rating) tornadoes, the number of significant tornadoes (>F2 rating), the DPI, the total path length of all tornadoes, the number of fatalities, the number of killer

tornadoes, and the number of tornadoes with track lengths >80 km (D06). Next, D06, beginning with days with seven or more tornadoes, detrended some of the aforementioned variables that exhibited temporal trends before computing the O index for outbreaks during the period 1970–2003. They also experimented with different weights (D06). Shafer and Doswell (2010a) took things a step further and developed a ranking system, for severe weather outbreaks from 1960–2006, that incorporates groups of variables with different weights. For example, their N17–N19 groups removed all but 2 of the tornado variables (Shafer and Doswell 2010a). Then, they separated their ranked outbreaks into “major,” “intermediate,” and “marginal” cases. For example, an event with an N15 index greater than 0.5 is classified as a major tornado outbreak. The categories’ loose correspondence to the Storm Prediction Center’s (SPC’s) categorical outlooks was also noted (Shafer and Doswell 2010a). This relation proved useful for the present study, since both criteria were used to define tornado outbreak thresholds.

Case Studies

Individual and regional tornado outbreaks have been widely researched. The Palm Sunday tornadoes of 1965 and the “Super Outbreak” of April 3, 1974 were a couple of the first outbreaks to be analyzed by multiple groups (Fujita et al. 1970). Agee et al. (1975) and Corfidi et al. (2010) provide synoptic and mesoscale analyses of the Super Outbreak. Another popularly studied outbreak is the May 3, 1999 outbreak in Oklahoma and Kansas. Among other publications, Thompson and Edwards (2000) and Edwards et al. (2002) gave an overview of

the outbreak and forecasting implications from an SPC perspective, while Roebber et al. (2002) explored synoptic-scale aspects of the outbreak. In addition, the outbreaks of March 21–22, 1952 and April 19, 1996 have been explored (Carr 1952, Lee et al. 2006). Still others cover regional outbreaks and outbreaks with similar characteristics (Hagemeyer 1977, Johns 1984, Schumacher and Boustead 2011).

Collectively, these studies can describe the synoptic-scale conditions most conducive to tornado outbreaks. Mercer et al. (2012), hereafter referred to as M12, provided a summary of these conditions. Most outbreaks occurred east of a surface low in environments containing a 500-hPa trough west of the low and an upper-level jet streak with one of its uplift regions collocated with the trough (M12). Additionally, Hamill et al. (2005) claimed the extended outbreak of May 3–11, 2003 followed the pattern outlined in Miller (1972) and Barnes and Newton (1983). This pattern adds the smaller-scale features of a southerly low-level jet in advance of a surface dryline and low pressure center (Hamill et al. 2005). The “Super Outbreak” of 1974 also exhibited this pattern (Corfidi et al. 2010). The April 19, 1996 outbreak occurred with a dryline but no low-level jet, lending further support to Hamill et al. (2005)’s claim (Lee et al. 2006).

A few outbreaks, however, do not follow these standard patterns. Maddox and Doswell (1982) warn that not all outbreaks are “synoptically apparent.” The 1994 Palm Sunday outbreak initiated due to a combination of mostly mesoscale processes (gravity waves, conditional symmetric instability, and a low-level jet) (Hales and Vescio 1996, Koch et al. 1998). Likewise, although most of the

synoptic-scale features for an outbreak were present on May 3, 1999, there was no apparent source of low-level uplift (Edwards et al. 2002). This uplift came in the form of a horizontal convective roll rather than typical synoptic-scale processes, similar to those of another outbreak on January 21 of that year (Thompson and Edwards 2000, Edwards et al. 2002).

Forecasting

Surprisingly, there is no literature focused solely on tornado outbreak forecasting. However, there has been some focus on SPC outbreak forecasting issues (Hales and Vescio 1996, Thompson and Edwards 2000, Edwards et al. 2002, Evans et al. 2008). Hales and Vescio (1996) emphasized the SPC's ability to forecast the 1994 Palm Sunday outbreak successfully despite its unusual synoptic-scale setup. The SPC recognized the mesoscale precursors to supercell formation and adjusted their outlooks accordingly (Hales and Vescio 1996). Due to numerical model inaccuracy preceding the May 3, 1999 outbreak, SPC forecasters were uncertain of the magnitude of convergence toward the dryline (Thompson and Edwards 2000, Edwards et al. 2002). Despite the classic synoptic-scale appearance of the event, the discrepancy in the numerical models and a large cirrus shield over the area east of the dryline led to a delayed identification of the substantial threat for tornadoes until the early afternoon of May 3; they upgraded their outlook to the highest risk level at 2000 UTC, 2 hours before the first significant (>F2) tornado (Thompson and Edwards 2000, Edwards et al. 2002). Thus, this would have been considered an event with low forecast

accuracy at a 12-hour forecast verification. Conversely, the outbreak of February 5, 2008 was synoptically apparent nearly a week before its occurrence and was therefore successfully forecasted by the SPC (Evans et al. 2008).

Compositing

Several studies have used composites to analyze synoptic-scale patterns associated with severe thunderstorms. Averaged composites have been used in a couple of national studies (Beebe 1956, Lowe and McKay 1962) and a few modern, regional ones (Hagemeyer 1997, Gaffin and Parker 2006, Wasula et al. 2007, Banacos and Ekster 2010). One study (Gaffin and Parker 2006) created these composites to analyze synoptic-scale patterns associated with significant tornado events. Averaging, however, has several limitations and can smooth out trough-ridge patterns, making significantly different systems appear similar (Beebe 1956, Schaefer and Doswell 1984, M12). These limitations call for the use of more advanced statistics.

Schaefer and Doswell (1984) used empirical orthogonal functions to create synoptic-scale map types of tornado outbreaks. However, their sample size was very small (14 outbreaks) and another statistical tool, rotated principal component analysis (RPCA, Richman 1986), has also been used for composite analyses such as those herein (Jones et al. 2004, M12, Richman and Mercer 2012). RPCA has several applications. Jones et al. (2004) used it to analyze a mesoscale detection algorithm and Richman and Mercer (2012) used it to identify intraseasonal modes of variability in 500-hPa geopotential heights. For the

purposes of this study, however, the application of RPCA to create synoptic-scale composites, found in M12, is the most relevant. Since M12 successfully discerned synoptic-scale differences between tornadic and nontornadic outbreaks using RPCA, this study can employ the same method to compare synoptic-scale conditions associated with tornado outbreaks with forecasts of varying accuracy.

Purpose of this Research

Work continues to be focused on synoptic-scale discrimination of tornadic and nontornadic outbreaks as well as ranking and identifying outbreak types. D06 laid the foundation for the research. Mercer et al. (2009), Shafer et al. (2009), and Shafer et al. (2010b) used D06's ranking scheme to choose the top 50 tornadic and primarily nontornadic outbreaks with which to assess the synoptic-scale variables best used to differentiate between the outbreaks. They found shear parameters were the most effective at separating the tornadic and nontornadic outbreaks; thermodynamic variables were the least effective. M12 concurred with the previous conclusion and noted the Weather Research and Forecasting (WRF) model's skill at discriminating between the two outbreak classes was adequate. The need for research into the "null" outbreaks where an outbreak was expected but did not occur has been expressed (Mercer et al. 2009, Shafer et al. 2010b, M12). The goal of taking their discrimination techniques operational has also been voiced (Mercer et al. 2009, Shafer et al.

2010b, M12). The present study seeks to take a step toward accomplishing these goals.

As mentioned previously, very little research has been performed on tornado outbreak forecasting. There has been some assessment of SPC outbreak forecasts (Hales and Vescio 1996, Thompson and Edwards 2000, Edwards et al. 2002, Evans et al. 2008), but, to the author's knowledge, no assessment of the factors associated with SPC forecasts of varying accuracy has been done. Preliminary research suggests that skill may not be high as it should be. This study sought to attempt to find ways to improve this skill by identifying possible problematic areas. This was done by determining synoptic-scale differences between SPC-forecasted outbreaks of varying accuracy.

CHAPTER II

DATA AND METHODS

Data

All non-tropical cyclone events from 2006-2012 for which the SPC convective outlook included a moderate categorical risk and a 10% tornado probability within 25 miles of a point at the Day 1, 13Z valid time were used in this study. The forecast polygons were obtained from an archived SPC tornado probability dataset. This project followed the same method as D06 by considering severe weather reports in separate 24-hour periods (1200 UTC on the outbreak day to 1159 UTC the following day). Composites of these events were created using NCEP/NCAR reanalysis data (Kalnay et al. 1996), global data defined on a 2.5º latitude-longitude grid with 17 vertical levels, from 1000 mb to 10 mb. The reanalysis variables that were analyzed include geopotential height, air temperature, specific humidity (SH), zonal and meridional wind components at all levels including the surface, sea level pressure (SLP), surface temperature, and surface specific humidity. Although most of these are based almost solely on observational data, with the exception of SH, that includes some model influence, the reanalysis dataset is still largely based on model output (Kalnay et al. 1996). It used assimilated surface data, model data, and remote sensing data to

parameterize the atmosphere (Kalnay et al. 1996). The domain used encompasses an outbreak-relative grid. The center of the outbreaks was determined using a centroid calculation on the SPC 10% tornado probability polygons. Finally, SPC tornado reports were used to assess the range of outbreak type (Schaefer and Edwards 1999).

Methods

Synoptic-scale conditions of 129 events between 2006 and 2012 for which the SPC forecasted tornado outbreaks, including “false alarm” events during which an outbreak was forecasted but did not materialize, were analyzed in this study. These events were chosen by perusing the SPC severe events archive (SPC 2014a, see example in Figure 1). (See Appendix A for a list of all events.) Since coastlines do not conform to simple polygons and there are very few, if any, tornado reports over bodies of water, all SPC polygons that adjoined large bodies of water were excluded from this project. This reduced the number of 10% tornado probability events from 161 to 129. For the purpose of this study, a tornado outbreak is defined as more than 6 reported tornadoes (D06).

To be consistent with the SPC policy of their probabilities being calculated 25 miles around a point, a 40-km buffer was implemented around the polygons. To create the buffer, the polygon points were first converted from spherical coordinates to Cartesian. The buffer was created by knowing, for a given line segment of the polygon, its slope is identical to the slope of the corresponding segment of the buffer and that the diagonal distance between the line segments

is the difference between the two lines' y-intercepts (see Figure 2 for an illustration). Then, Δb can be found using the equation:

$$\Delta b = \frac{40\ km}{\cos(\theta)} \tag{1}$$

where Δb is the difference between the lines y-intercepts and θ is the angle between the diagonal and horizontal lines between the polygon side and the buffer. The y-intercept of the buffer line segment is thus the y-intercept of the polygon's line segment added to Δb, and the buffer's line equation is found from there. Finally, the intersecting points of these segments were found and became a vertex of the new polygon. Repeating this process for each line segment that made up the polygon created the buffer. See an example of a buffered polygon in Figure 3.

Before the numbers of tornado reports within the polygons were determined, the report coordinates were converted to Cartesian to facilitate comparison to the buffered polygons. Following this, a point-in-polygon algorithm found the number of reports within the polygons. The point-in-polygon algorithm determined if a point was within a polygon by summing the angles between the point and the edge of the polygon. If the angle was 360°, the point was considered inside the polygon. These sums were then converted to percentages of reports within a polygon. By making a histogram of these percentages, a distribution of outbreak forecast accuracy was created (Figure 4). For example, the far right side of the distribution indicates that there were more than 6 tornado reports within an SPC 10% tornado probability polygon and no or very few

reports outside of it, an indication of 100% forecast accuracy (see Figure 5 for more examples). This distribution was then divided into quartiles, in order of increasing forecast accuracy. The quartiles (hereafter referred to as Q1-4) were bounded at 42.9%, 70%, and 87.5% forecast accuracy (Figure 4). The first quartile held 27 events and the second, third, and fourth all had 26 events each. There were 24 events in the false alarm (FA) group that were analyzed separate from the distribution. Hereafter, each of the four quartiles and the FA group will be referred to as a QF.

From the QFs, variables from the NCEP/NCAR reanalysis dataset (Kalnay et al. 1996) were used to create composites using rotated principal component analysis (RPCA), a methodology employed by M12 that is explained below. A few common meteorological parameters, like advections and wind magnitudes, were computed to further assess the synoptic setups. The composites were created for timesteps 24 hours prior to the collective outbreak time to the onset of the outbreak. (All outbreak valid times are taken to be 0000 UTC the day after the outbreak, as in M12). In addition, to remove spatial biases, the composites were centered on each outbreak by calculating the centroid of the SPC tornado probability polygons and centering the composite domain on the nearest reanalysis gridpoint to the centroid.

RPCA is a subset of principal component analysis (PCA). The process of PCA begins with the equation:

$$\mathbf{Z} = \mathbf{F}\,\mathbf{A}^{\mathbf{T}} \tag{2}$$

where **Z** is a standardized anomaly matrix of the input data, **F** is a matrix of principal component (PC) scores, and **A** is a matrix of PC loadings (Wilks 2009). **F** is a transformation of **Z** such that the columns in **F** are uncorrelated. The loading matrix **A** is used to transform the original data into the uncorrelated score data, or vice versa. It is a linear combination of the terms in **F** that can be used to reproduce **Z**. Also, **A**'s columns are in order of decreasing variability explained of **Z** (M12). Additionally, these columns are the weights used to recreate the linear combination and determine **Z**.

Before determining the PC scores and loadings, the data in **Z** are standardized. Usually, this involves removing the mean and dividing by each variable's standard deviation, creating standard anomalies. Since the variables cover several vertical levels and have different magnitudes, each variable at each level was converted separately (M12).

Next, a correlation matrix of **Z**, **R,** is computed. However, RPCA contains different modes that are performed at this step depending on what end product the user wants. For the present study, composites of the atmospheric variables are desired. This leaves S and T modes, as defined by Richman (1986). Since variability between the outbreaks is the topic of this study, T mode is chosen, as it correlates along the time dimension—the outbreaks, in this case (M12). This correlation was performed using the equation:

$$\mathbf{R} = \frac{\mathbf{Z}^T\mathbf{Z}}{n-1} \tag{3}$$

Following, **R** is diagonalized into an eigenvalue matrix **D** with an associated eigenvector matrix **V** through the equation:

$$\mathbf{R = V\,D\,V}^{T} \tag{4}$$

By definition, eigenvectors point in directions of maximum variability within a dataset. Therefore, a small subset of the original eigenvalues associated with **V** might describe most of the important variability in **Z.** To exclude eigenvalues with low variability, **V** was truncated before the final computation of **F** is completed so only the eigenvalues that include the most variability are retained. **V** was truncated using the congruence coefficient (Richman and Lamb 1985), defined as:

$$\eta = \frac{\sum xy}{\sqrt{\sum x^2 \sum y^2}} \tag{5}$$

where x is the vector of the correlation matrix that corresponds to the largest magnitude loading for a given loading vector, and y is the loading vector. If the value of η was less than 0.81 for a given loading, that loading was dropped (M12).

The truncated **V** and **D** matrices are then used to calculate the loading matrix **A** from the equation**:**

$$\mathbf{A = V\,D}^{1/2} \tag{6}$$

The largest eigenvalue is associated with the first principal component (PC). It always describes the greatest variability in the dataset. Likewise, subsequent eigenvalues describe lower variability. However, the associated eigenvectors may not point in the direction of the greatest variability; due to their orthogonality,

they may point between local variability maxima. To circumvent this issue, a Varimax PC rotation (Richman 1986) further rotates the coordinate system (M12). This provides a new rotated loading matrix **B** that accounts for the same total variance explained as in **A** and has the same dimensionality as **A**. In addition, the formation of **B** spreads the explained variance throughout the rotated principal components (M12).

Finally, **B** was used to create composite maps of each scenario. This matrix represents the weights in a linear combination of the **F** matrix that reproduce the most variance in **Z.** In other words, the rotated loadings represent the relationship between the individual outbreaks for each scenario and **F** (M12). In order to facilitate comparison, the rotated loadings with similar magnitudes must be grouped together. A hierarchical cluster analysis using Ward's method was run to group the similar loadings (see example in Figure 6). This created 4 map types for each QF (Figure 7). Then, the similar loadings were averaged together, creating an averaged composite of the similar PCs. Finally, the randomly-ordered map types were analyzed for similarities within each QF and then compared to the other groups.

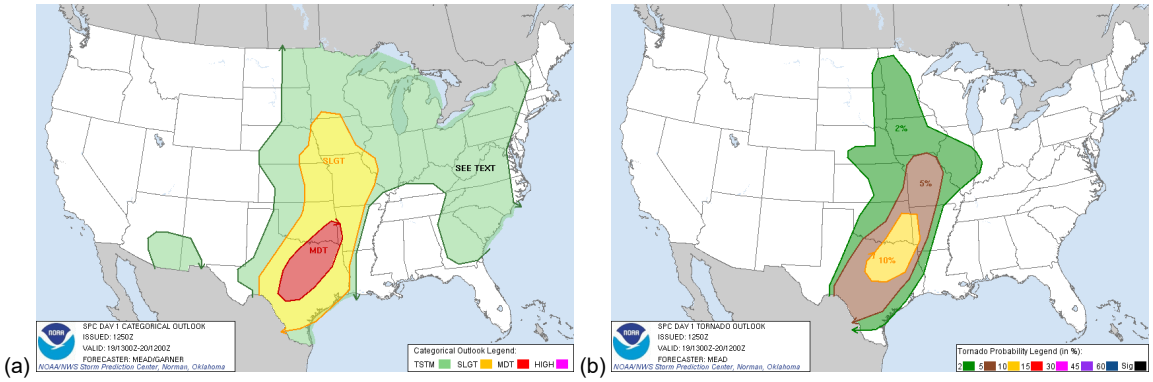

Figure 1 Example Event with Moderate Risk and 10% Tornado Probability

(a) Categorical moderate risk from March 19, 2012
(b) Tornado probabilities from March 19, 2012

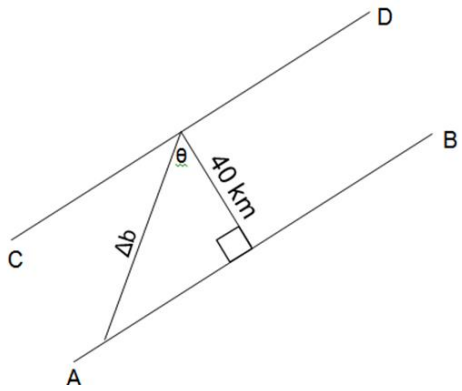

Figure 2 Illustration of Buffer Methodology

Note: $\overline{CD}$ is the original polygon and $\overline{AB}$ is the buffer. Also, $\overline{CD}$ and $\overline{AB}$ are parallel and their slopes are identical.

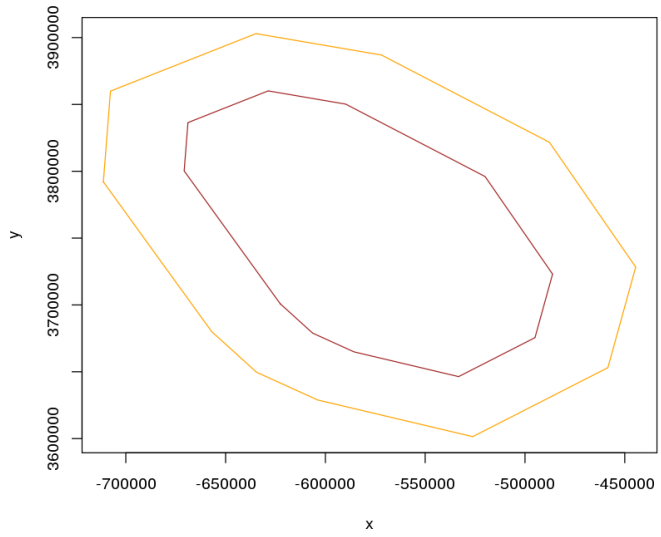

Figure 3 Illustration of Buffered Polygon (orange) versus the Original (brown)

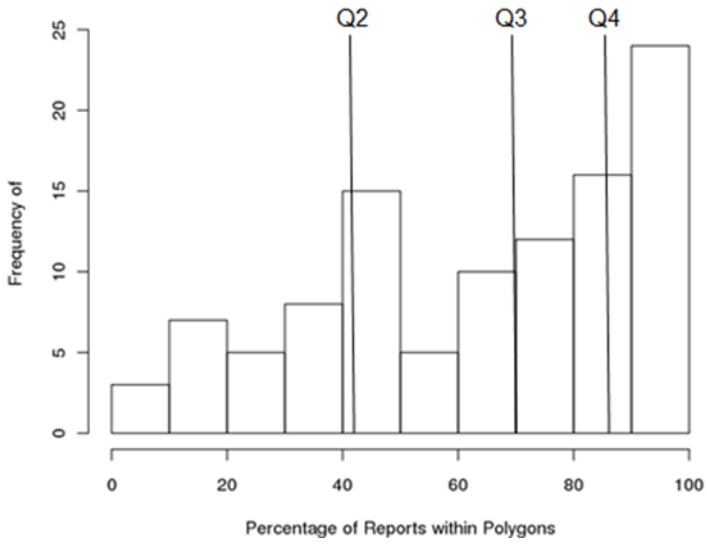

Figure 4 Percentage of Tornado Reports inside SPC 10% Tornado Probabliity Polygons with Quartiles Identified

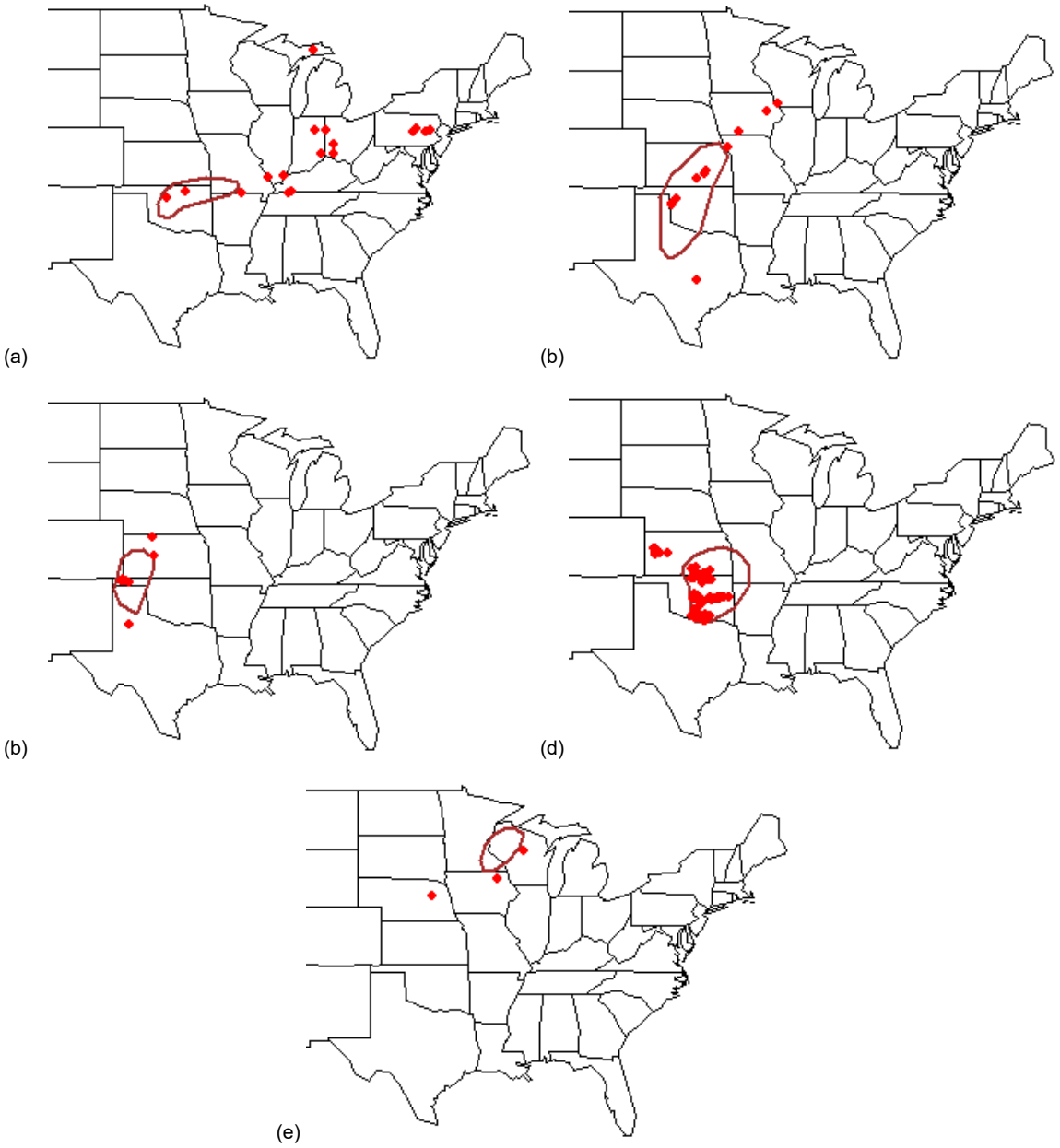

Figure 5 Sample Events from Each QF

(a) Q1 example, May 23, 2011
(b) Q2 example, April 26, 2009
(c) Q3 example, May 31, 2007
(d) Q4 example, May 10, 2010
(e) FA example, May 24, 2012

Note: These are the actual forecasted polygons; they are not buffered.

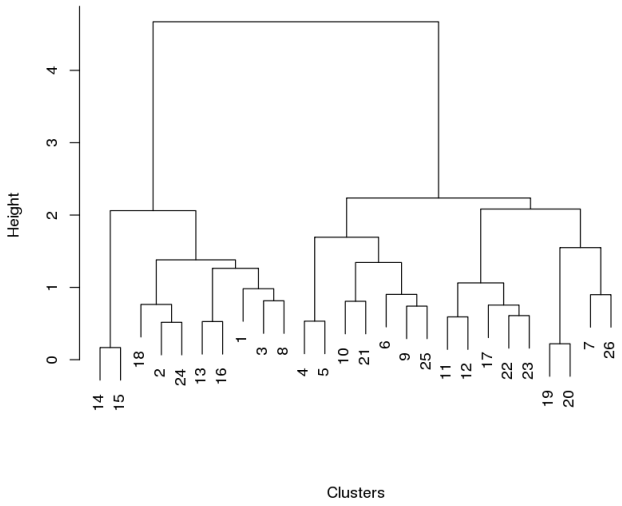

Figure 6 Example Dendrogram Used to Determine 4 Map Types for Q2

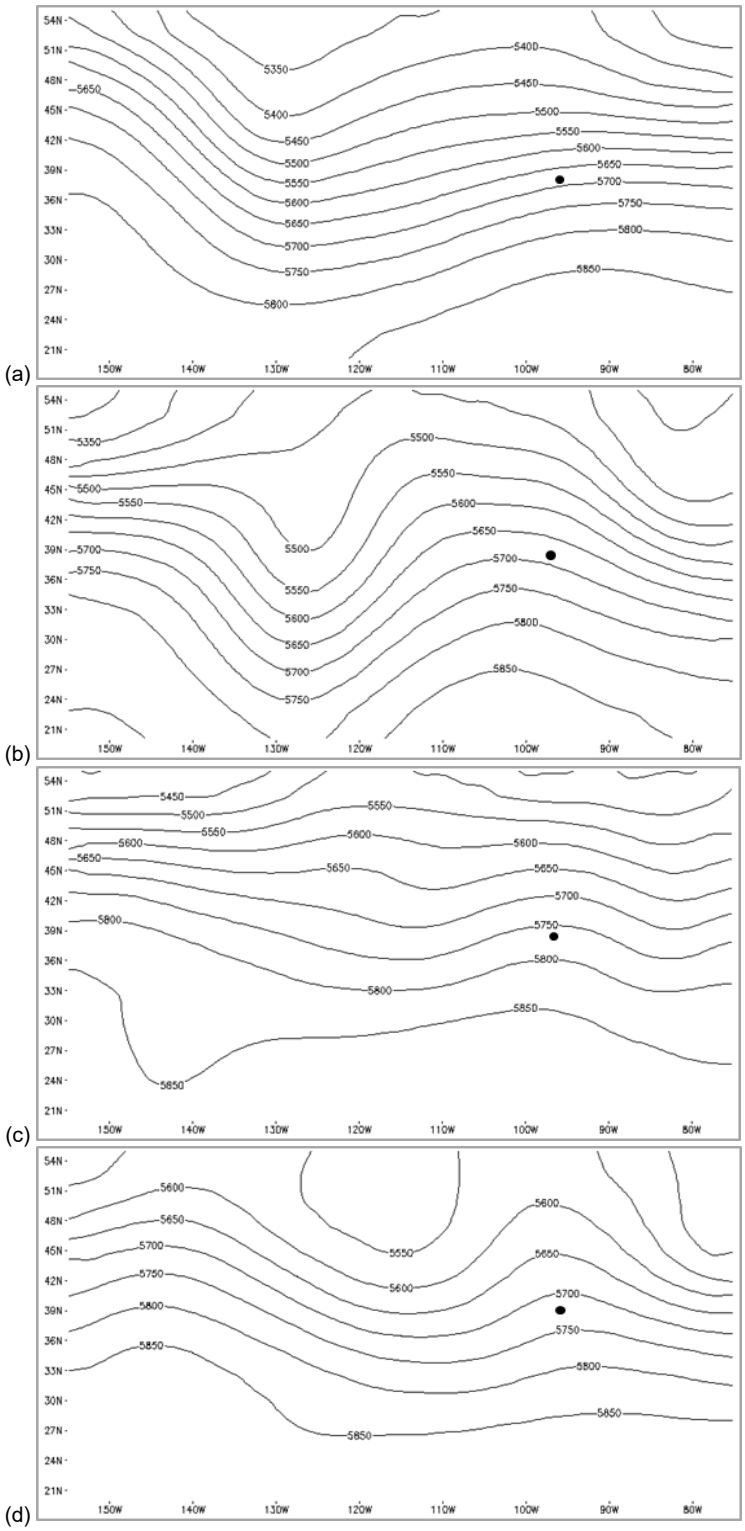

Figure 7 Sample Map Types from Q4 of 500 hPa Height (m) at 24 Hours before Outbreak Time

CHAPTER III

RESULTS AND DISCUSSION

Composites of several synoptic-scale variables are displayed on maps to facilitate visual comparison between them. However, since these composites are outbreak-relative, the geographic location of the displayed features is irrelevant (M12). To achieve a better look at conditions upstream of the outbreaks, the domain was extended to the West. Therefore, the outbreaks occur on the right side of the composites. The latitudes and longitudes are provided for distance reference only. Also note that actual values may be less than normal since they have been averaged.

The most basic means to measure strength of weather systems is pressure. At the 500 hPa level, the orientations of the QF troughs vary. The troughs in the map types for Q1 were all positively- or neutrally-tilted at 24 hours prior to the outbreak and at the onset of the outbreak. Q2's troughs ranged from both positively- and negatively-tilted at 24 hours prior to the outbreak to mostly neutrally-tilted at outbreak time (Figure 8). The troughs in Q3's map types displayed all variations of tilt prior to the outbreak time but were all neutral by the outbreak's onset. Q4's troughs transitioned from neutrally- to positively-tilted by outbreak time. Finally, the troughs in the FA group's map types ranged from

positively-tilted to mostly zonal 24 hours prior to the outbreak to negatively-tilted to mostly zonal at the time of the outbreak.

As there is no favorable tilt for tornado outbreak formation, these varying results are not surprising. M12 found tornado outbreaks occur across all 3 tilts. Outbreaks have occurred with various trough phases, as the April 27, 2011 outbreak occurred with a negatively-tilted trough (Knupp et al. 2013) but the troughs associated with the outbreaks in the Southern Appalachians study exhibited positive tilts (Gaffin and Parker 2006). Additionally, it is reasonable to assume that the FA group's troughs were positively-tilted and strong 24 hours prior to the outbreak but weakened or sped up before the outbreak occurred. Furthermore, their more zonal appearance may be an indication of their inability to produce a tornado outbreak. In contrast, the troughs of Q4 are an anomaly. Instead of displaying the common evolution of troughs from positively- to negatively-tilted, they portray a backwards progression from neutral to positive (Figure 9). This could have been caused by a shortwave trough moving through the region, which is not uncommon in tornado outbreak occurrences. The April 3, 1974 and May 3, 1999 tornado outbreaks both included shortwave impulses that temporarily enhanced some of the convection (Agee et al. 1975, Thompson and Edwards 2000, Edwards et al. 2002, Roebber et al. 2002, Corfidi et al. 2010). Another discrepancy of these height fields as a whole is they did not exhibit mostly zonal flow elsewhere, as described in the literature (Fujita et al. 1970, Agee et al. 1975, M12).

The sea level pressure observation painted a different picture. The SLP at the time of the outbreak is shown in Figure 10 for each QF using the map type that most represents the cluster. The surface low in Q1 was around 1008 hPa and deepened to about 1006 hPa. Q2's low strengthened from 1009 to 1007 hPa. The low in Q3 is a bit stronger, ranging from 1007 hPa 24 hours prior to the outbreak to 1004 hPa at the time of the outbreak. Q4's low is again average with a pressure of 1010 hPa deepening to 1007 hPa by outbreak time. Surprisingly, the FA surface low is nearly identical to that of the Q4 low. These results indicate SLP is not a good distinguisher between correctly- and incorrectly-forecasted outbreaks. All of the surface lows marginally strengthen over the analyzed time period and they are all of about the same strength. They are even visually similar, as seen from the relatively high correlation coefficients in Table 1.

Temperature advection is another important meteorological quantity to assess (Figure 11). It was analyzed 6 hours prior to the time the outbreak occurred to distinguish the amount of energetic warm air moving into the area and the strength of the cold air advection (CAA) behind the surface trough. Q1's and Q2's map types exhibited widespread areas of warm air advection (WAA) of about 5×10^{-5} K s^{-1} and CAA of a similar magnitude. Q3, as with its SLP, displayed the strongest WAA and CAA, with both having magnitudes of 8×10^{-5} K s^{-1}. Q4 had a broad area of strong WAA and a small and slightly weaker area of CAA. The FA group's WAA was fairly weak and its CAA was comparatively stronger and more widespread. Furthermore, the low correlation coefficients in Table 2 show the QFs' temperature advections were spatially dissimilar.

These temperature advection results are interesting. The quartiles with high forecast accuracy (Q3 and Q4) appear to have WAA of double the strength and slightly weaker CAA than the low-accuracy QF (Q1, Q2, and FA). The weak WAA in Q1 and Q2 could have been one of the reasons these outbreaks were under-forecasted or misplaced. In addition, the lack of strong WAA in the FA cases could have been overshadowed by other factors favorable for tornado outbreaks when the forecast was being created, and thus one of the limiting factors of the non-events.

As tornado outbreaks cannot form without sufficient moisture aloft, specific humidity was also analyzed (not shown). As in the case of the SLP, the specific humidities were similar and unchanging across the QFs and timesteps (Table 3). The values ranged from 0.003 to 0.004 kg kg^{-1}. The highest values were, as expected, along the Gulf Coast and in the warm sector ahead of the trough. Specific humidity does not appear to be a distinguishing variable.

Since they are associated with regions of enhanced uplift crucial for thunderstorm formation, jet streaks were assessed at 300 hPa. There were no significant differences in their orientations. Most of the jet streaks in every QF flowed from southwest to northeast, almost paralleling the height contours (see Figure 12). Most of the streaks were 35-40 m s^{-1} in strength. These strengths were consistent with the other results of this study, with Q3 having the strongest jet and Q1 and FA being about 25% weaker (Figure 13). The outbreaks largely occurred in the right exit regions, a known area of subsidence. Although this is a surprising result, Rose et al. (2004) states that, on their outbreak days, 73%

more tornadoes occurred in the right exit region than in the right entrance, a known area of uplift. Also, a study on Southern Appalachian tornadoes found that half of their outbreaks occurred in right exit regions (Gaffin and Parker 2006). Maddox and Doswell (1982) also credit the notion of severe thunderstorm formation in “regions not usually considered favorable.”

Relative vorticity, a very important mesoscale factor in tornado formation, is also important on the synoptic scale. The relative vorticity maxima associated with the QFs’ 500 hPa troughs ranged from 2×10^{-5} s^{-1} to 5×10^{-5} s^{-1}. However, the strengths do not coincide with previous results. Although the FA group has the weakest relative vorticity maxima, Q2 has the strongest (not shown). An important factor to consider is the amount of positive relative vorticity being advected, known as differential positive vorticity advection (DPVA), since it indicates quasigeostrophic uplift if present at 500 hPa. Figure 14 shows Q2 has the strongest DPVA 6 hours before the outbreak occurred while Q1 and FA have the weakest. The FA group was expected to have the weakest, as nontornadic outbreaks are known to have weaker DPVA than tornado outbreaks (M12). However, these advections do not correspond with the SLP results, showing DPVA was not the main cyclogenetic forcing mechanism for these events. As shown by the quasigeostrophic omega equation, DPVA and WAA both provide uplift, but the term that “wins” varies by event. Since thermal advection had the most significant distinction between the QFs, it is possible it could have been the main cyclogenetic factor in these cases.

Vertical wind shear distinguishes supercellular structures from multicellular if it is above about a 20 m s^{-1} threshold in the roughly 850-300 hPa layer (Markowski and Richardson 2010). All but one of the QFs, Q1, had shear above this threshold. As seen in Figure 15, the spatial distribution of Q1's shear is very similar to the other QFs', which here is represented by Q4. The only difference between them is the magnitude of the shear—Q4's shear is 27% stronger than Q1's. It is possible the outbreaks represented by Q1 were able to initiate in low-shear environments, which has happened on occasion. For instance, a small outbreak occurred on March 23, 2007 with shear values as low as 15 m s^{-1} (SPC 2014). Additionally, as low level shear is essential for tornado formation, it is interesting to note that Q4's 1000-700 hPa shear was significantly (~5 m s^{-1}) stronger than Q1's, yet tornadoes were still able to form in the Q1 events. However, it is possible that Q1's low shear could simply be a product of the smoothing involved in the compositing process.

Low-level jets (LLJs) can act to enhance vertical wind shear and thus were observed at 850 hPa (not shown). They ranged from 6-11 m s^{-1} across the QFs, with the FA group having the weakest LLJs. Almost all of the LLJs were oriented from southwest to northeast, similar to the 300-hPa jet streaks. Since their magnitudes are not much different from the surface winds and their orientations do not differ from the jet streaks', these LLJs did not enhance vertical wind shear very much in the mid-levels. Again, the PCA and averaging resulting in weaker values could be the reason for this result. However, it enhanced directional wind

shear in the lowest portion of the atmosphere since most of the surface winds across the QFs ranged from southerly to southeasterly.

Lapse rates, that give an estimate of how unstable an air mass is, were computed. Lapse rates through the 1000-500 hPa layer underwent a weighted average, resulting in an average lapse rate for the layer. The lapse rates were very similar across the QFs, only ranging from -6.4 K km^{-1} to -6.2 K km^{-1} (not shown). Again, Q3 had the strongest lapse rates. This time, Q1 and Q2 had the weakest. However, as these values are between the moist adiabatic lapse rate of 6 K/km (SPC 2014c) and the accepted "steep" lapse rate of 7 K/km (Craven 2000), they are not representative of most tornado outbreaks. Their small magnitude is most likely a result of the sparse vertical spatial resolution and the averaging. Nevertheless, their almost identical magnitudes across the QFs suggest lapse rates are not a good identifier of tornadic outbreaks. As the literature has documented thermodynamic variables' ineptness at discriminating between tornadic and nontornadic outbreaks (Mercer et al. 2009, Shafer et al. 2009, Shafer et al. 2010b, M12), this result makes sense.

Finally, surface conditions are also significant features of environments favorable for tornado outbreak formation. Surface temperature, specific humidity, and winds were all analyzed (not shown). The surface temperatures were all very similar, spanning 294-300 K (21-24°C) in the warm sectors across the QFs. They were spatially similar as well, as seen from their correlation matrix (Table 4). Likewise, the surface specific humidity values were nearly identical, with 0.009-0.01 kg kg^{-1} being the highest values, and sharp gradients behind the troughs.

These statements are supported by the correlation matrix in Table 5 that shows high correlation coefficients across the QF. The surface winds were also very comparable, averaging around 5 m s^{-1} and southerly-southeasterly in the warm sectors, converging toward their corresponding surface cold fronts.

Altogether, this study does not show many apparent, significant differences between synoptic setups of the SPC-forecasted events with low and high forecast accuracy. However, it can be noted that the events with low forecast accuracy, the ones in Q1 and the FA group, for the most part, consistently had the weakest supercell-supportive environments. Q1's result is reasonable, since the events in that quartile could have been synoptically ambiguous. It is likely those events were determined by mesoscale processes rather than synoptic-scale ones. In the example Q1 case shown in Figure 4a, the 0Z OUN sounding showed a cap was still present and the level of free convection (LFC) was almost 1000 m higher than the LFC on the ILN sounding (SPC 2014a). ILN's cap had eroded, unlike OUN's (SPC 2014a) Therefore, the environment was not as conducive to tornado formation as forecasters expected at OUN and it was more conducive at ILN, due to mesoscale processes. It was surprising, however, that the FA group's parameters did not weaken just prior to the outbreak but instead were weak during the duration of the 24-hour period. In the case of the example in Figure 4e, ample synoptic-scale uplift was present and the 12Z MPX sounding showed sufficient bulk Richardson number (BRN) shear and storm-relative helicity (SRH) for supercell formation but marginal CAPE and CIN (SPC 2014a). Its 0Z sounding revealed the CAPE had been

eradicated and the favorable SRH was gone, leaving the environment insufficient for supercell formation in that case (SPC 2014a). It appears that, again, mesoscale processes were the deciding factors in FA cases.

Table 1 Sea Level Pressure Correlation Matrix

	Q1	Q2	Q3	Q4	FA
Q1	1.0000000	0.8943434	0.8346462	0.8588869	0.7170988
Q2	0.8943434	1.0000000	0.8900068	0.8450857	0.8327374
Q3	0.8346462	0.8900068	1.0000000	0.8718789	0.8311016
Q4	0.8588869	0.8450857	0.8718789	1.0000000	0.7565252
FA	0.7170988	0.8327374	0.8311016	0.7565252	1.0000000

Table 2 Temperature Advection Correlation Matrix

	Q1	Q2	Q3	Q4	FA
Q1	1.0000000	0.3995634	0.5710137	0.7622895	0.4289083
Q2	0.3995634	1.0000000	0.3074189	0.5197709	0.1286094
Q3	0.5710137	0.3074189	1.0000000	0.6438575	0.3591432
Q4	0.7622895	0.5197709	0.6438575	1.0000000	0.4871903
FA	0.4289083	0.1286094	0.3591432	0.4871903	1.0000000

Table 3 Specific Humidity (kg kg^{-1}) for All Timesteps and QFs

Time	Q1	Q2	Q3	Q4	FA
24 hrs prior	0.0035	0.003	0.003	0.0027	0.0035
18 hrs prior	0.0035	0.003	0.003	0.0025	0.0035
12 hrs prior	0.0035	0.003	0.0035	0.0027	0.0035
6 hrs prior	0.004	0.003	0.0035	0.0027	0.0037
Outbreak time	0.004	0.0033	0.0035	0.0003	0.0035

Table 4 Surface Temperature Correlation Matrix

	Q1	Q2	Q3	Q4	FA
Q1	1.0000000	0.9311069	0.9564582	0.9026532	0.9119759
Q2	0.9311069	1.0000000	0.9272045	0.9175449	0.7831311
Q3	0.9564582	0.9272045	1.0000000	0.9562306	0.8990379
Q4	0.9026532	0.9175449	0.9562306	1.0000000	0.8561713
FA	0.9119759	0.7831311	0.8990379	0.8561713	1.0000000

Table 5 Surface Specific Humidity Correlation Matrix

	Q1	Q2	Q3	Q4	FA
Q1	1.0000000	0.8743458	0.9650301	0.9507761	0.9036280
Q2	0.8743458	1.0000000	0.8412573	0.8905133	0.7257472
Q3	0.9650301	0.8412573	1.0000000	0.9386608	0.9223100
Q4	0.9507761	0.8905133	0.9386608	1.0000000	0.9051036
FA	0.9036280	0.7257472	0.9223100	0.9051036	1.0000000

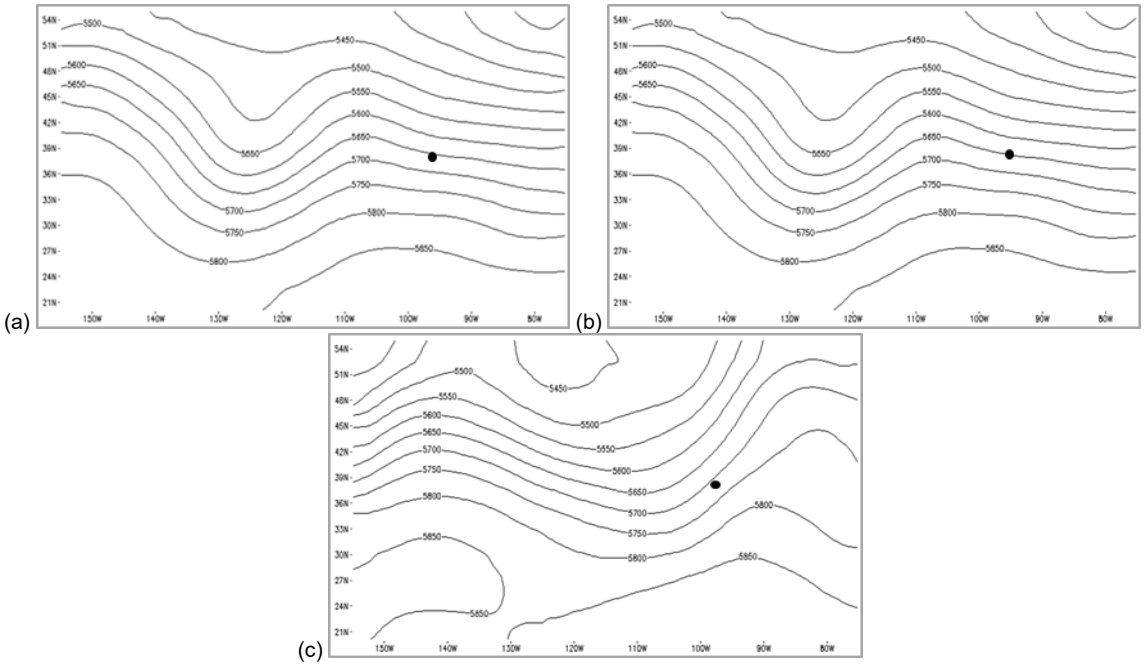

Figure 8 Examples of Trough Orientations from Q2

(a) Cluster 1, 24 hours prior to outbreak
(b) Cluster 2, 24 hours prior to outbreak
(c) Cluster 1, at outbreak time

(a) 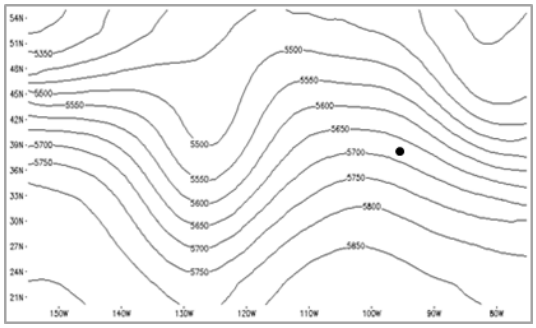 (b) 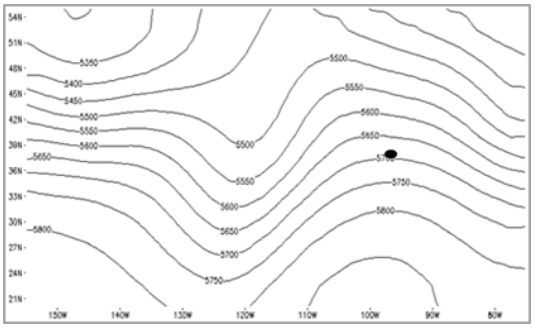

Figure 9 Example of Q4 500 mb Heights (m)

(a) 24 hours prior to outbreak
(b) at outbreak time

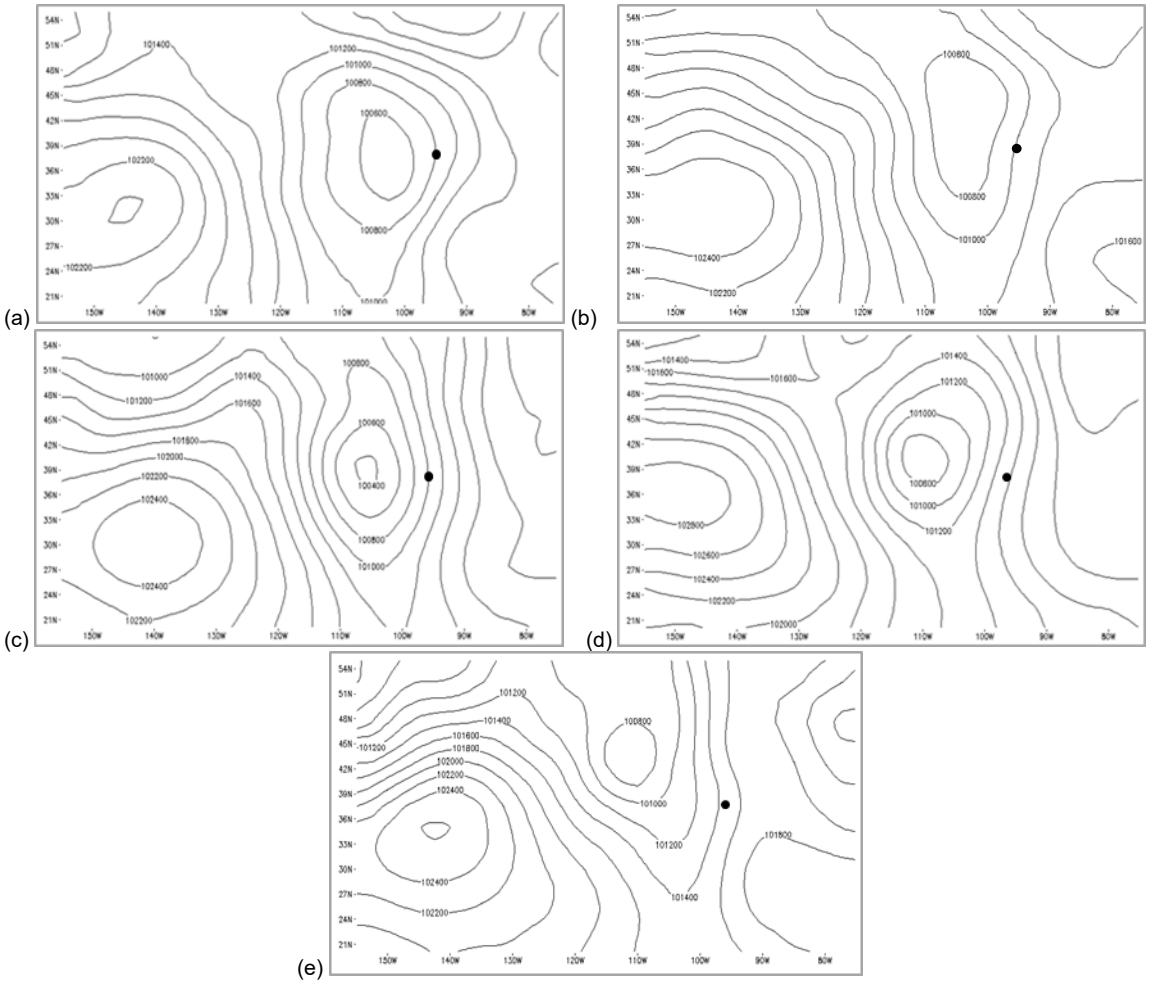

Figure 10 SLP (hPa) from Most Representative Map Type at Outbreak Time for Each QF

(a) Q1 map type 3
(b) Q2 map type 3
(c) Q3 map type 1
(d) Q4 map type 1
(e) FA map type 1

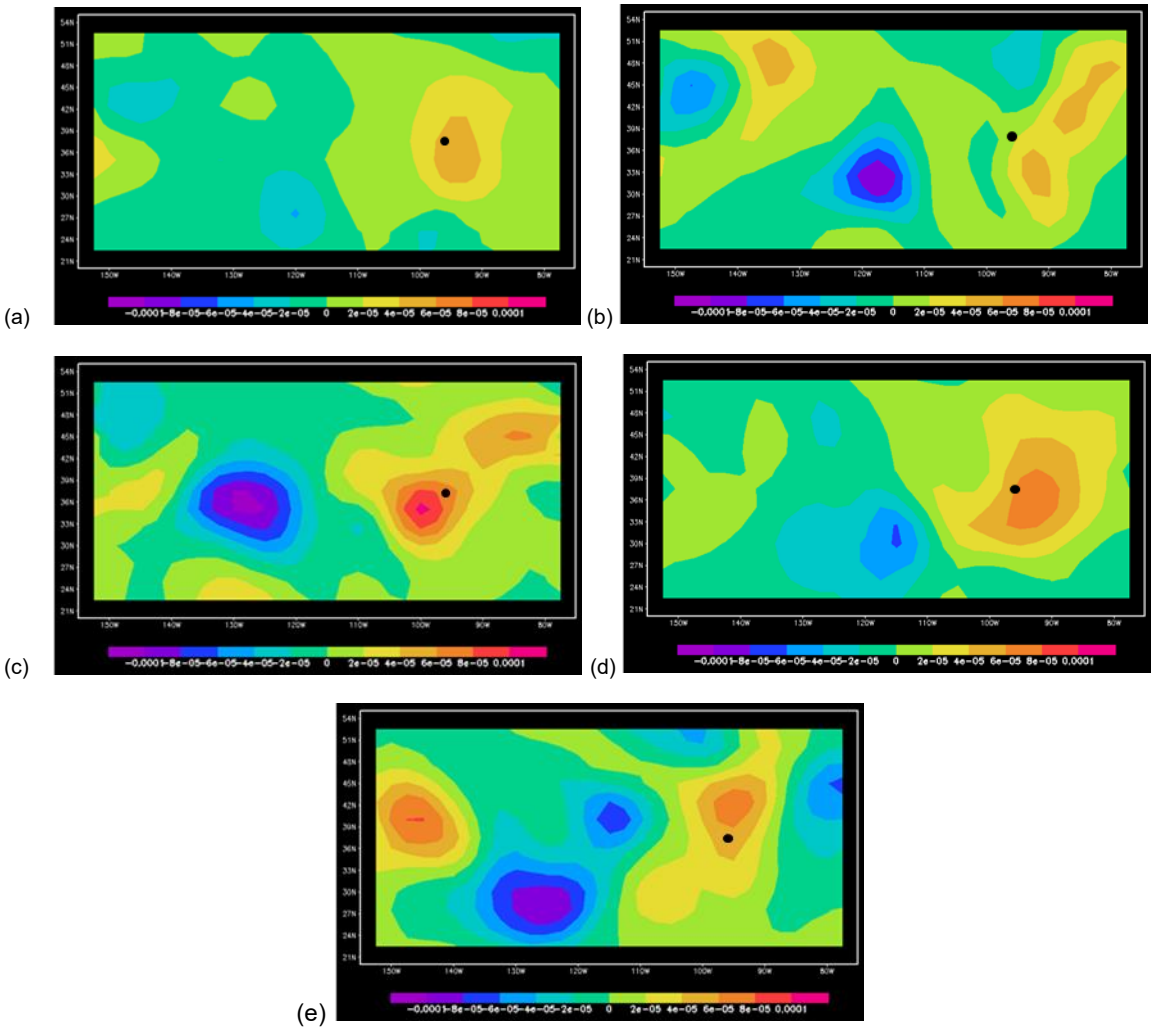

Figure 11 Temperature Advection (K s^{-1}) 6 Hours Prior to Outbreak at 850 hPa for Each QF

(a) Q1 map type 3
(b) Q2 map type 2
(c) Q3 map type 4
(d) Q4 map type 2
(e) FA map type 3

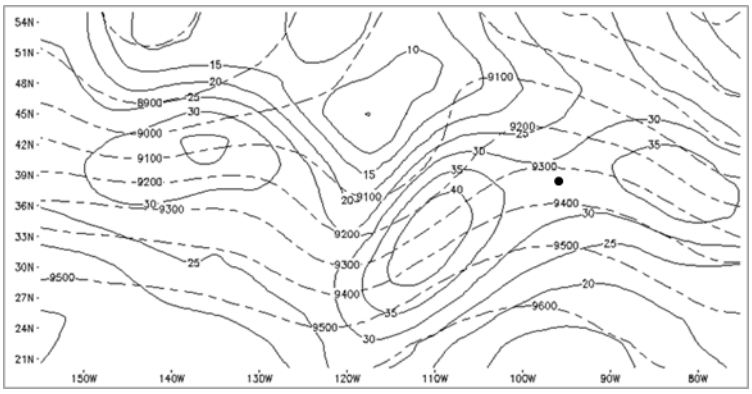

Figure 12 300 hPa Wind Speeds (m s^{-1}, solid lines) and Height (m, dashed lines) at Outbreak Time for Q4 Map Type 2

(a) 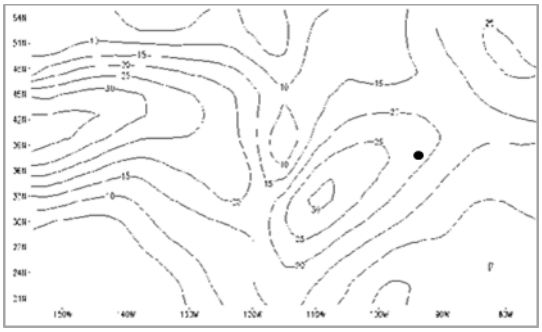 (b) 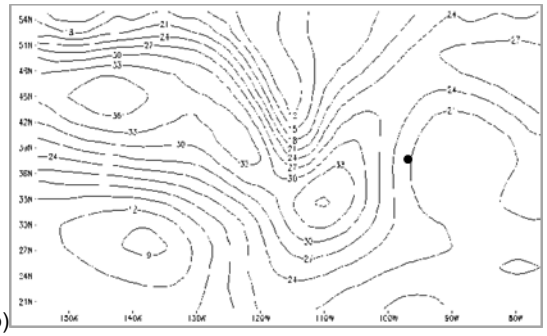

Figure 13 300 hPa Wind Speeds (m s^{-1}) at Outbreak Time for Q1 and Q3

(a) Q1 map type 3
(b) Q3 map type 1

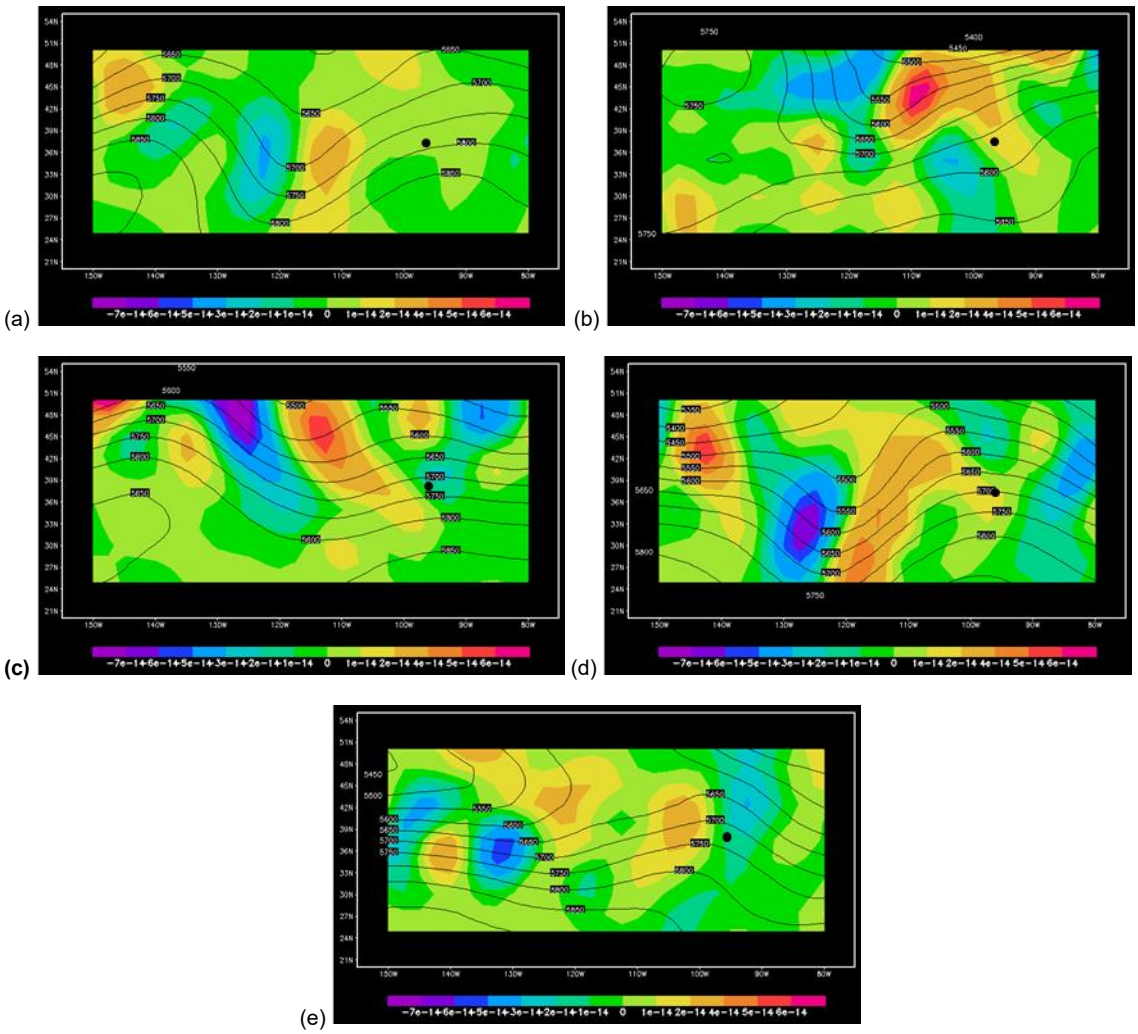

Figure 14 Differential Vorticity Advection (s^{-2} Pa^{-1}, shaded) and Height (m, solid lines) at 500 hPa for Each QF

(a) Q1 map type 3
(b) Q2 map type 4
(c) Q3 map type 2
(d) Q4 map type 2
(e) FA map type 3

(a) 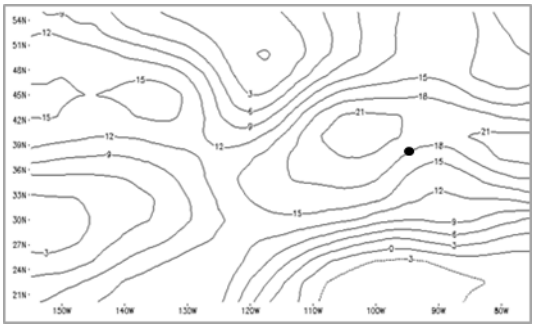 (b) 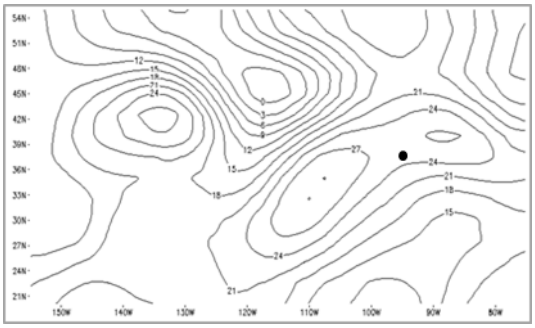

Figure 15 850-300 hPa Vertical Wind Shear (m s^{-1}) for Q1 and Q4

(a) Q1 map type 1
(b) Q4 map type 2

CHAPTER IV

SUMMARY AND CONCLUSIONS

Tornadic events and non-events for which the Storm Prediction Center issued forecasts of varying accuracy were analyzed for synoptic-scale differences. Composites of common synoptic-scale variables were created using rotated principal component analysis and cluster analyses on NCEP/NCAR reanalysis data. Temperature and differential vorticity advection, jet streak magnitudes, and vertical wind shear were the variables with the most noticeable differences. Pressure, wind speeds, and moisture aloft and at the surface, as well as lapse rates and surface temperature, were nearly identical amongst the QF. However, Q3 consistently had the strongest synoptic-scale variables and Q1 and the FA group had the weakest setups.

These results indicate that the objectives for this project have been met and the hypothesis can be accepted. Although there were not many, there were some synoptic-scale differences that suggest some variables may be good indicators of low-accuracy tornado outbreak forecasts. These could prove useful for operational tornado outbreak forecasting. First, the differing thermal advections could be used. They suggest that a lack of incoming warm air could be taken as an indication of insufficient energy or, from quasigeostrophic theory,

a lack of uplift, to create tornado outbreaks in false alarm cases, or that the outbreak may be displaced or more widespread in the case of Q1 events. It is also possible that the WAA was simply over-forecasted for these events. Nonetheless, M12 also noted stronger thermal advection with tornadic rather than nontornadic outbreaks.

Other parameters showed notable differences. The vertical wind shear results signify that days with weak or moderate shear may result in more widespread outbreaks. Moreover, the weak DPVA in Q1 and the FA group could be indicative of weaker quasi-geostrophic forcing in these cases, as also indicated by the weak WAA. In contrast to the FA group's, the DPVA in Q1's case is organized and positioned close to the surface low, signaling a veering wind profile that suggests a curved hodograph and strong helicity, possibly giving more support to the idea of a wider outbreak than forecasted (as was evident in the Q1 cases, see below). Finally, Q1 and the FA group's weak jet streaks are further evidence of those groups' weak synoptic setups.

The overall weaker conditions of Q1 and the FA group show that the SPC's low-accuracy forecasts are associated with days with synoptic-scale conditions that were indistinguishable with regard to tornado outbreak formation, resulting in considerable forecast uncertainty. In the future, forecasters could be wary of weak synoptic setups, especially those with limited WAA, vertical wind shear, and DPVA. Some even say WAA could be more important than DPVA where uplift for severe storms is concerned and that it should be given more attention by forecasters (Maddox and Doswell 1982). Furthermore, upon closer

inspection of the actual Q1 events, only about 25% of these were completely missed forecasts. The remainder happened to be more widespread outbreaks than forecasted. It is possible, then, that the averaged weaker conditions could be spread over a large area, providing a larger environment conducive to tornado formation. Thus, forecasters could also pay attention to days with weak yet broad tornado-favorable synoptic-scale conditions.

It should also be noted that the QFs exhibited seasonal patterns (Figure 16). The FA group and especially Q1 events were almost fully divided between meteorological spring and summer, while the Q3 and Q4 events occurred mainly in the spring. It is not surprising that all the QFs had most of their outbreaks in the spring, but a significant observation can be made about summer. Most of the summertime outbreaks fall in the low-accuracy forecast QFs (Q1, Q2, and the FA group). Nontornadic outbreaks are known to be sensitive to seasonality (Shafer et al. 2009, Shafer et al. 2010b). Hence, it is possible that forecasters focused on a nontornadic outbreak setup and underestimated tornadic potential during the Q1 and Q2 events. Additionally, most of the fall events fell into the FA group, possibly because of the pre-conceived notion of a “secondary” tornado season in the fall. These observations show that non-tornado season outbreaks are an area of forecast uncertainty and more research is needed to determine synoptic-scale parameters associated with outbreaks outside of spring to assist forecasters in recognizing them.

These conclusions are contingent upon the many limitations associated with this study. They include calculation, data, and human error. The problems

with the tornado report database that were described in Chapter I apply, as well as time discrepancies between the SPC's severe events archive (SPC 2014a) and its tornado report database (SPC 2014b). Another factor to consider is this study assumed there was no subjectivity with the SPC's tornado probability forecasts. There was also some error involved in the creation of the buffers around the forecast polygons; the polygons were converted to Cartesian coordinates to apply the buffers. Then, the tornado reports were converted to Cartesian to facilitate comparison. Finally, as mentioned previously, the RPCA and associated averaging smoothed out some of the extremes and resulted in lower than average values for the analyzed variables.

There is still work to be done, but evidence of significant synoptic-scale differences between tornadic and nontornadic outbreaks is being discovered. The work in this study, M12, and others is laying groundwork for synoptic-scale processes to become more integral to tornado outbreak forecasting and their results will be shared with the SPC to assist in their forecasting procedures. Additional future work in this area includes inputting the cases analyzed in this study into the Weather Research and Forecasting model to assess its ability to use synoptic-scale variables to discriminate between these forecasts. There are also plans to make composites of all documented tornado outbreaks and to compare hail and wind composites to tornado composites.

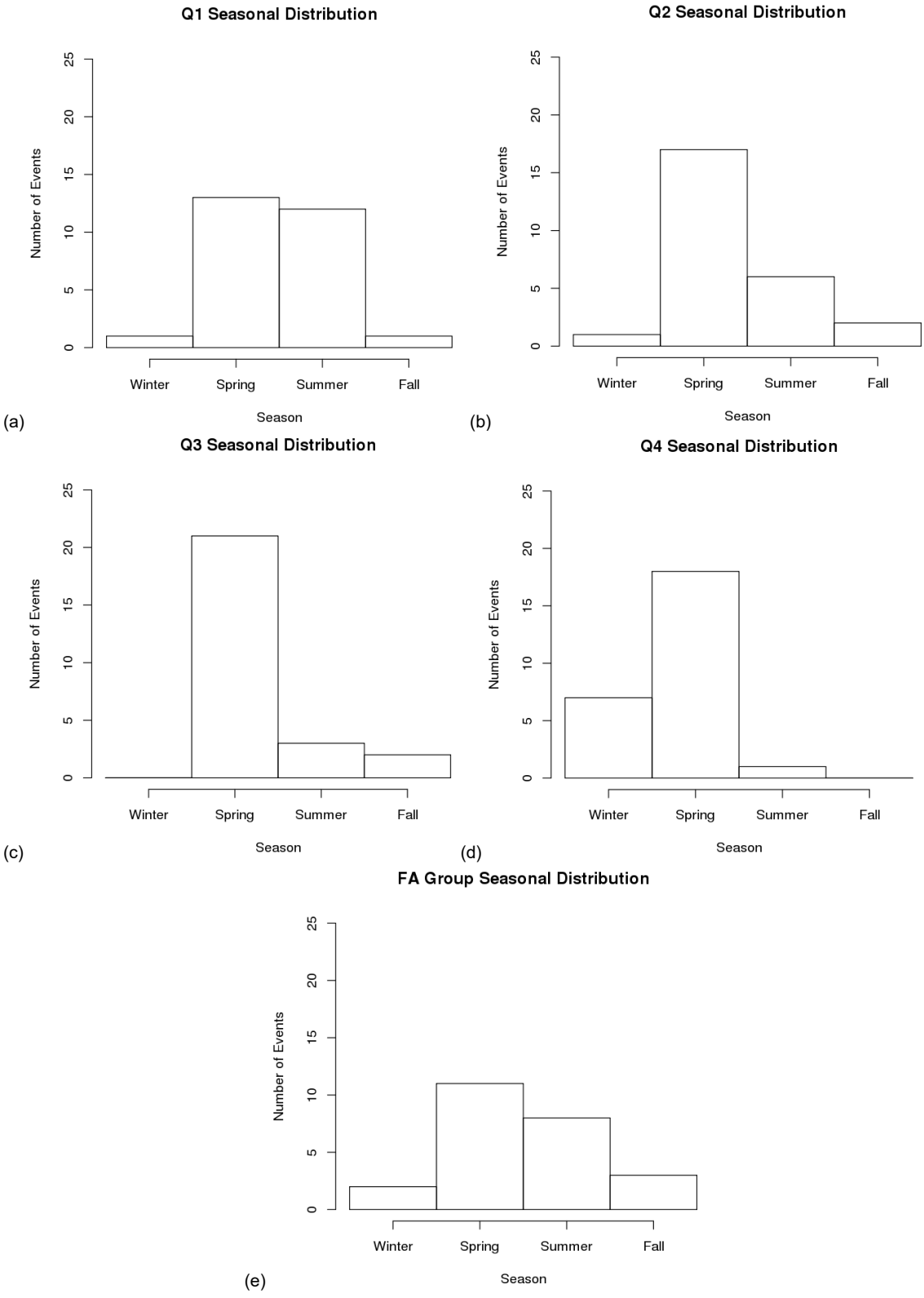

Figure 16 Number of Events per Season for Each QF

BIBLIOGRAPHY

Agee, E., C. Church, C. Morris, and J. Snow, 1975: Some synoptic aspects and dynamic features of vortices associated with the tornado outbreak of 3 April 1974. *Mon. Wea. Rev.*, **103**, 318-333. doi: 10.1175/1520-0493(1975)103<0318:SSAADF>2.0.CO;2

Banacos, P. C. and M. L. Ekster, 2010: The association of the elevated mixed layer with significant severe weather events in the northeastern United States. *Wea. Forecasting*, **25**, 1082–1102. doi: 10.1175/2010WAF2222363.1

Beebe, R. G., 1956: Tornado composite charts. *Mon. Wea. Rev.*, **84**, 127–142. doi: 10.1175/1520-0493(1956)084<0127:TCC>2.0.CO;2

Blunden, J., and D. S. Arndt, 2012: State of the climate in 2011. *Bull. Amer. Meteor. Soc.*, **93**, S1–S282. doi: 10.1175/2012BAMSStateoftheClimate.1

Brooks, H. E., C. A. Doswell, and M. P. Kay, 2003: Climatological estimates of local daily tornado probability for the United States. *Wea. Forecasting*, **18**, 626–640. doi: 10.1175/1520-0434(2003)018<0626:CEOLDT>2.0.CO;2

Carr, J. A., 1952. A preliminary report on the tornadoes of March 21-22, 1952. *Mon. Wea. Rev.*, **80**, 50-58. doi: 10.1175/1520-0493(1952)080<0050:APROTT>2.0.CO;2

Cook, A. R., J. T. Schaefer, 2008: The relation of El Niño–Southern Oscillation (ENSO) to winter tornado outbreaks. *Mon. Wea. Rev.*, **136**, 3121–3137. doi: 10.1175/2007MWR2171.1

Corfidi, S., S. Weiss, J. Kain, S. Corfidi, R. Rabin, and J. Levit, 2010: Revisiting the 3-4 April 1974 Super Outbreak of Tornadoes. *Wea. Forecasting*, **25**, 465-510. doi: 10.1175/2009WAF2222297.1

_____, 2013: Notable American tornado outbreaks and thoughts on some local events. The 2013 National Storm Conference, Colleyville, TX, Texas Severe Storms Association.

Craven, J. P., 2000: A preliminary look at deep layer shear and middle level lapse rates during major tornado outbreaks. *Preprints*. 20th Conf. on Severe Local Storms, 11-15 September 2000, Orlando, Amer. Meteor. Soc., 547-550.

Doswell, C. A., and D. W. Burgess, 1988: On some issues of United States tornado climatology. *Mon. Wea. Rev.*, **116**, 495–501. doi: 10.1175/1520-0493(1988)116<0495:OSIOUS>2.0.CO;2

_____, R. Edwards, R. L. Thompson, J. A. Hart, and K. C. Crosbie, 2006: A simple and flexible method for ranking severe weather events. *Wea. Forecasting*, **21,** 939–951. doi: 10.1175/WAF959.1

_____, 2007: Small sample size and data quality issues illustrated using tornado occurrence data. *Electronic J. Severe Storms Meteor*., 2 (5), 1–16.

Edwards, R., S. F. Corfidi, R. L. Thompson, J. S. Evans, J. P. Craven, J. P. Racy, D. W. McCarthy, M. D. Vescio, 2002: Storm Prediction Center forecasting issues related to the 3 May 1999 Tornado Outbreak. *Wea. Forecasting*, **17**, 544–558. doi: 10.1175/1520-0434(2002)017<0544:SPCFIR>2.0.CO;2

_____, R. L. Thompson, K. C. Crosbie, J. A. Hart, and C. A. Doswell III, 2004: A proposal for modernized definitions of tornado and severe thunderstorm outbreaks. Preprints, *22d Conf. on Severe Local Storms,* Hyannis, MA, Amer. Meteor. Soc., 7B.2.

Evans, J. S., C. M. Mead, and S. J. Weiss, 2008: Forecasting the Super Tuesday tornado outbreak at the Storm Prediction Center: Why forecast uncertainty does not necessarily decrease as you get closer to a high impact weather event. *Preprints*, 24th Conf. Severe Local Storms, Savannah, GA, 3A.2.

Fujita, T., D. L. Bradbury, and C. F. Van Thullenar, 1970: Palm Sunday tornadoes of April 11, 1965. *Mon. Wea. Rev.*, **98**, 29-69. doi: 10.1175/1520-0493(1970)098<0029:PSTOA>2.3.CO;2

_____, 1981: Tornadoes and downbursts in the context of generalized planetary scales. *J. Atmos. Sci.*, **38**, 1511–1534. doi: 10.1175/1520-0469(1981)038<1511:TADITC>2.0.CO;2

Gaffin, D. M., and S. S. Parker, 2006: A climatology of synoptic conditions associated with significant tornadoes over the southern Appalachian region. *Wea. Forecasting*, **21**, 735-751. doi: 10.1175/WAF951.1

Galway, J. G., 1977. Some climatological aspects of tornado outbreaks. *Mon. Wea. Rev.*, **105**, 477-484. doi: 10.1175/1520-0493(1977)105<0477:SCAOTO>2.0.CO;2

Gao, J., J. Tang, C. Fu, D. C. Dowell, and D. J. Stensrud, 2012: 3DVAR analysis and forecast experiments for the 27 April 2011 tornado outbreak. Preprints, *26th Conf. on Severe Local Storms,* Nashville, TN, Amer. Meteor. Soc., 7.2.

Glickman, T., S., Ed., 2000: Glossary of Meteorology. 2nd ed. Amer. Meteor. Soc., 782 pp.

Hagemeyer, B., 1997: Peninsular Florida tornado outbreaks. *Wea. Forecasting*, **12**, 399-427. doi: 10.1175/1520-0434(1997)012<0399:PFTO>2.0.CO;2

Hamill, T. M., R. S. Schneider, H. E. Brooks, G. S. Forbes, H. B. Bluestein, M. Steinberg, D. Meléndez, R. M. Dole, 2005: The May 2003 extended tornado outbreak. *Bull. Amer. Meteor. Soc.*, **86**, 531–542. doi: 10.1175/BAMS-86-4-531

Hayes, J.. L, 2011: The historic tornadoes of April 2011. U.S. Department of Commerce Service Assessment. 76 pp.

Hitchens, Nathan M., Harold E. Brooks, 2012: Evaluation of the Storm Prediction Center's Day 1 Convective Outlooks. *Wea. Forecasting*, **27**, 1580–1585. doi: http://dx.doi.org/10.1175/WAF-D-12-00061.1

Johns, R., 1984: A synoptic climatology of northwest-flow severe weather outbreaks. Part II: Meteorological parameters and synoptic patterns. *Mon. Wea. Rev.*, **112**, 449-464. doi: 10.1175/1520-0493(1984)112<0449:ASCONF>2.0.CO;2

Jones, T. A., K. M. McGrath, and J. T. Snow, 2004: Association between NSSL mesocyclone detection algorithm-detected vortices and tornadoes. *Wea. Forecasting*, **19**, 872–890. doi: 10.1175/1520-0434(2004)019<0872:ABNMDA>2.0.CO;2

Kalnay, E., M. Kanamitsu, R. Kistler, W. Collins, D. Deaven, L. Gandin, M. Iredell, S. Saha, G. White, J. Woolen, Y. Zhu, A. Leetmaa, B. Reynolds, M. Chelliah, W. Ebisuzaki, W. Higgins, J. Janowiak, K. C. Mo, C. Ropelewski, J. Wang, R. Jenne, and D. Joseph, 1996. The NCEP/NCAR 40-Year Reanalysis Project. *Bull. Amer. Meteor. Soc.*, **77**, 437-471. doi: 10.1175/1520-0477(1996)077<0437:TNYRP>2.0.CO;2

Kelly, D. L., J. T. Schaefer, R. P. McNulty, C. A. Doswell, R. F. Abbey, 1978: An augmented tornado climatology. *Mon. Wea. Rev.*, **106**, 1172–1183. doi: 10.1175/1520-0493(1978)106<1172:AATC>2.0.CO;2

Knupp, K. R., T. A. Murphy, T. A. Coleman, R. A. Wade, S. A. Mullins, C. J. Schultz, E. V. Schultz, L. Carey, A. Sherrer, E. W. McCaul Jr., B. Carcione, S. Latimer, A. Kula, K. Laws, P. T. Marsh, and K. Klockow, 2013: Meteorological overview of the devastating 27 April 2011 tornado outbreak, *Bull. Amer. Meteor. Soc.*, e-View. doi: 10.1175/BAMS-D-11-00229.1

Koch, S. E., D. Hamilton, D. Kramer, and A. Langmaid, 1998: Mesoscale dynamics in the Palm Sunday Tornado Outbreak. *Mon. Wea. Rev.*, **126**, 2031–2060. doi: 10.1175/1520-0493(1998)126<2031:MDITPS>2.0.CO;2

Lee, B. D., B. F. Jewett, and R. B. Wilhelmson, 2006: The 19 April 1996 Illinois Tornado Outbreak. Part I: Cell evolution and supercell isolation. *Wea. Forecasting*, **21**, 433-448. doi: 10.1175/WAF944.1

Lowe, A. B., and G. A. McKay, 1962: Tornado composite charts for the Canadian Prairies. *J. Appl. Meteor.*, **1**, 157-162. doi: 10.1175/1520-0450(1962)001<0157:TCCFTC>2.0.CO;2

Maddox, Robert A., and C. A. Doswell, 1982: An examination of jet stream configurations, 500 hPa vorticity advection and low-level thermal advection patterns during extended periods of intense convection. *Mon. Wea. Rev.*, **110**, 184–197. doi: 10.1175/1520-0493(1982)110<0184:AEOJSC>2.0.CO;2

Markowski, P., and Y. Richardson, 2010: *Mesoscale Meteorology in Midlatitudes*. Wiley-Blackwell, 407 pp.

Mercer, A. E., C. M. Shafer, C. A. Doswell, L. M. Leslie, and M. B. Richman, 2009: Objective classification of tornadic and nontornadic severe weather outbreaks. *Mon. Wea. Rev.*, **137**, 4355-4368. doi: 10.1175/2009MWR2897.1

_____, C. M. Shafer, C. A. Doswell, L. M. Leslie, and M. B. Richman, 2012: Synoptic composites of tornadic and nontornadic outbreaks. *Mon. Wea. Rev.*, **140**, 2590–2608. doi: 10.1175/MWR-D-12-00029.1

Pautz, M. E., 1969: Severe local storm occurrences, 1955–1967. ESSA Tech. Memo. WBTM FCST12, Washington, DC, 77 pp.

Richman, M. B., and P. J. Lamb, 1985: Climatic pattern analysis of three- and seven-day summer rainfall in the central United States: Some methodological considerations and a regionalization. *J. Climate Appl. Meteor.*, **24**, 1325–1343. doi: http://dx.doi.org/10.1175/1520-0450(1985)024<1325:CPAOTA>2.0.CO;2

_____, 1986: Rotation of principal components. *J. Climatology*, **6**, 293-335. doi: 10.1002/joc.3370060305

_____, and A. E. Mercer, 2012: Identification of intraseasonal modes of variability using rotated principal components. *Chapter 12. Atmospheric Model Applications,* I. Yucel, Ed.*,* Intech*,* 273-296.

Roebber, P., D. Schultz, and R. Romero, 2002: Synoptic regulation of the 3 May 1999 tornado outbreak. *Wea. Forecasting*, **17,** 399-429. doi: 10.1175/1520-0434(2002)017<0399:SROTMT>2.0.CO;2

Rose, S. F., P. V. Hobbs, J. D. Locatelli, M. T. Stoelinga, 2004: A 10-yr climatology relating the locations of reported tornadoes to the quadrants of upper-level jet streaks. *Wea. Forecasting*, **19**, 301–309. doi: http://dx.doi.org/10.1175/1520-0434(2004)019<0301:AYCRTL>2.0.CO;2

Schaefer, J., and C.A. Doswell III, 1984: Empirical orthogonal function expansion applied to progressive tornado outbreaks. *J. Meteor. Soc. Japan*, **62**, 929-936.

_____, and R. Edwards, 1999: The SPC tornado/severe thunderstorm database. Preprints, *11th Conf. on Applied Climatology*, Dallas, TX, Amer. Meteor. Soc., 603–606.

Schumacher, P. N., and J. M. Boustead, 2011: Mesocyclone evolution associated with varying shear profiles during the 24 June 2003 tornado outbreak. *Wea. Forecasting*, **26**, 808–827. doi: 10.1175/WAF-D-10-05021.1

Shafer, C. M., A. E. Mercer, C. A. Doswell, M. B. Richman, and L. M. Leslie, 2009: Evaluation of WRF forecasts of tornadic and nontornadic severe weather outbreaks when initialized with synoptic scale input. *Mon. Wea. Rev.*, **137**. 250-1271. doi: 10.1175/2008MWR2597.1

_____, and C. A. Doswell III, 2010a: A multivariate index for ranking and classifying severe weather outbreaks. *Electronic J. Severe Storms Meteor.,* **5** (1), 1–39.

_____, A. E. Mercer, L. M. Leslie, M. B. Richman, and C. A. Doswell, 2010b: Evaluation of WRF model simulations of tornadic and nontornadic outbreaks that occur in the spring and fall. *Mon. Wea. Rev.*, **138**, 4098-4119. doi: 10.1175/2010MWR3269.1

_____, and C. A. Doswell III, 2011: Using kernel density estimation to identify, rank, and classify severe weather outbreak events. *Electronic J. Severe Storms Meteor.,* **6** (2)**,** 1–28.

Storm Prediction Center, cited 2014: SPC severe weather events archive. [Available online at http://www.spc.noaa.gov/exper/archive/events/.]

Storm Prediction Center, cited 2014: Storm Prediction Center WCM page [Available online at http://www.spc.noaa.gov/wcm/#data.]

Storm Prediction Center, cited 2014: Lapse rate. [Available online at http://www.spc.noaa.gov/sfctest/help/help_lllr.html.]

Thompson, R.L., and M.D. Vescio, 1998. The Destruction Potential Index - a method for comparing tornado days. Preprints, 19th Conf. Severe Local Storms, Amer. Meteor. Soc., Minneapolis, MN, 280-282.

_____, Roger Edwards, 2000: An overview of environmental conditions and forecast implications of the 3 May 1999 Tornado Outbreak. *Wea. Forecasting*, **15**, 682–699. doi: 10.1175/1520-0434(2000)015<0682:AOOECA>2.0.CO;2

Verbout, Stephanie M., Harold E. Brooks, Lance M. Leslie, David M. Schultz, 2006: Evolution of the U.S. Tornado Database: 1954–2003. *Wea. Forecasting*, **21**, 86–93. doi: 10.1175/WAF910.1

Wasula, A. C., L. F. Bosart, R. Schneider, S. J. Weiss, R. H. Johns, G. S. Manikin, and P. Welsh, 2007: Mesoscale aspects of the rapid intensification of a tornadic convective line across central Florida: 22–23 February 1998. *Wea. Forecasting*, **22**, 223–243. doi: 10.1175/WAF977.1

Wilks, D. S., 2009. *Statistical Methods in the Atmospheric Sciences*. Academic Press, 627 pp.

APPENDIX A

LIST OF EVENT DATES

Table 4 Event Dates Organized by QF

Q1	Q2	Q3	Q4	FA
April 28, 2006	March 11, 2006	March 9, 2006	March 12, 2006	Feb. 16, 2006
May 2, 2006	March 20, 2006	March 30, 2006	April 6, 2006	March 8, 2006
May 9, 2006	April 2, 2006	April 10, 2006	April 7, 2006	April 1, 2006
August 24, 2006	April 23, 2007	May 10, 2006	April 15, 2006	April 18, 2006
Sept. 16, 2006	April 24, 2007	Sept. 22, 2006	Feb. 24, 2007	April 24, 2006
April 4, 2007	May 6, 2007	March 28, 2007	Feb. 28, 2007	May 25, 2006
April 10, 2008	October 17, 2007	April 13, 20007	March 23, 2007	July 19, 2006
April 24, 2008	April 23, 2008	April 21, 2007	May 23, 2007	Sept. 23, 2006
June 4, 2008	May 22, 2008	May 4, 2007	February 5, 2008	Nov. 14, 2006
March 23, 2009	May 25, 2008	May 5, 2007	April 3, 2008	Feb. 23, 2007
March 27, 2009	June 7, 2008	May 31, 2007	April 9, 2008	March 25, 2007
May 5, 2009	June 11, 2008	March 31, 2008	May 23, 2008	June 6, 2007
June 7, 2009	April 9, 2009	May 2, 2008	May 29, 2008	June 16, 2007
June 6, 2009	April 25, 2009	May 10, 2008	Dec. 9, 2008	May 13, 2008
June 17, 2009	April 26, 2009	June 3, 2008	Feb. 10, 2009	May 31, 2008
June 19, 2009	May 13, 2009	June 5, 2008	April 10, 2009	June 18, 2009
June 20, 2010	June 15, 2009	June 6, 2010	May 1, 2010	June 10, 2010
June 22, 2010	April 23, 2010	October 26, 2010	May 10, 2010	April 3, 2011
June 26, 2010	May 10, 2010	April 9, 2011	July 14, 2010	June 26, 2011
July 17, 2010	May 19, 2010	April 19, 2011	Feb. 24, 2011	April 27, 2012
Feb. 27, 2011	May 24, 2010	April 25, 2011	April 10, 2011	May 25, 2012
May 23, 2011	June 17, 2010	April 26, 2011	April 14, 2011	June 14, 2012
June 20, 2011	June 25, 2010	April 27, 2011	April 15, 2011	June 17, 2012
July 26, 2011	Feb. 28, 2011	May 24, 2011	Feb. 29, 2012	Sept. 8, 2012
March 19, 2012	June 19, 2011	May 25, 2011	March 2, 2012	
April 15, 2012	Sept. 5, 2011	May 30, 2011	April 14, 2012	
May 30, 2012				